# Hypoxia-inducible factor 1α activates insulin-induced gene 2 (Insig-2) transcription for degradation of 3-hydroxy-3-methylglutaryl (HMG)-CoA reductase in the liver

Received for publication, March 27, 2017, and in revised form, April 14, 2017 Published, Papers in Press, April 17, 2017, DOI 10.1074/jbc.M117.788562

**Seonghwan Hwang[‡], Andrew D. Nguyen[‡], Youngah Jo[‡], Luke J. Engelking[‡], James Brugarolas[§], and Russell A. DeBose-Boyd[‡1]**

*From the [‡]Department of Molecular Genetics and [§]Simmons Comprehensive Cancer Center, University of Texas Southwestern Medical Center, Dallas, Texas 75390-9046*

Edited by George M. Carman

**Cholesterol synthesis is a highly oxygen-consuming process. As such, oxygen deprivation (hypoxia) limits cholesterol synthesis through incompletely understood mechanisms mediated by the oxygen-sensitive transcription factor hypoxia-inducible factor 1α (HIF-1α). We show here that HIF-1α links pathways for oxygen sensing and feedback control of cholesterol synthesis in human fibroblasts by directly activating transcription of the *INSIG-2* gene. Insig-2 is one of two endoplasmic reticulum membrane proteins that inhibit cholesterol synthesis by mediating sterol-induced ubiquitination and subsequent endoplasmic reticulum-associated degradation of the rate-limiting enzyme in the pathway, HMG-CoA reductase (HMGCR). Consistent with the results in cultured cells, hepatic levels of Insig-2 mRNA were enhanced in mouse models of hypoxia. Moreover, pharmacologic stabilization of HIF-1α in the liver stimulated HMGCR degradation via a reaction that requires the protein's prior ubiquitination and the presence of the Insig-2 protein. In summary, our results show that HIF-1α activates *INSIG-2* transcription, leading to accumulation of Insig-2 protein, which binds to HMGCR and triggers its accelerated ubiquitination and degradation. These results indicate that HIF-mediated induction of Insig-2 and degradation of HMGCR are physiologically relevant events that guard against wasteful oxygen consumption and inappropriate cell growth during hypoxia.**

A pair of endoplasmic reticulum (ER)-localized[2] membrane proteins called Insig-1 and Insig-2 mediate two feedback-regulatory mechanisms that converge on the ER membrane protein 3-hydroxy-3-methylglutaryl coenzyme A reductase (HMGCR), which catalyzes a rate-limiting step in the synthesis of cholesterol and nonsterol isoprenoids, including farnesyl pyrophosphate and geranylgeranyl pyrophosphate (1). One of these mechanisms involves the sterol-accelerated, ER-associated degradation (ERAD) of HMGCR (2, 3). This ERAD is initiated by the intracellular accumulation of sterols such as the cholesterol biosynthetic intermediate 24,25-dihydrolanosterol (24,25-DHL) (4–6), which triggers binding of Insigs to the membrane domain of HMGCR (3). Insig-associated ubiquitin ligases subsequently facilitate the ubiquitination of two cytosolically exposed lysine residues in the membrane domain of HMGCR (7, 8), marking it for membrane extraction and proteasome-mediated ERAD (9).

The second mechanism through which Insigs mediate feedback control of HMGCR involves modulating the activation of membrane-bound transcription factors called sterol regulatory element-binding proteins (SREBPs) (1). This activation requires the escort protein Scap, which mediates transport of SREBPs from the ER to the Golgi for the proteolytic release of transcriptionally active fragments from membranes. Upon release, these fragments migrate to the nucleus, where they activate the transcription of genes encoding HMGCR and other enzymes required for cholesterol synthesis (10). Insigs inhibit the proteolytic activation of SREBPs through their sterol-induced binding to Scap. Insig binding traps Scap and its associated SREBP in the ER, thereby preventing access of SREBPs to Golgi-localized proteases (1). Thus, the levels of mRNAs encoding SREBP target genes fall, and cholesterol synthesis declines. Together, these Insig-mediated reactions (sterol-induced ER retention of Scap-SREBP and sterol-accelerated ERAD of HMGCR) ensure that cells maintain production of essential nonsterol isoprenoids while avoiding overaccumulation of cholesterol or one of its sterol precursors.

The two Insig proteins share ~60% amino acid sequence identity and appear to be functionally redundant (2, 11, 12). Topology studies of Insig-1 indicate that the protein contains six transmembrane helices separated by short loops, with both the N and C termini facing the cytosol (13). The degree of sequence similarity to Insig-1 indicates that Insig-2 is similarly oriented in ER membranes. Despite these similarities, Insig-1 and Insig-2 are differentially regulated in the mouse liver. The Insig-1 gene is a target gene of SREBP, and its mRNA varies according to the amount of SREBP in the nucleus (12, 14). Two

* This work was supported by National Institutes of Health Grants HL020948 (to R. A. D. B.), CA196516 (to J. B.), and DK102652 (to L. J. E.). J. B. is a member of the Scientific Advisory Board for Bethyl Laboratories. The content is solely the responsibility of the authors and does not necessarily represent the official views of the National Institutes of Health.

This article contains supplemental Figs. 1 and 2 and Tables 1–4.

[1] To whom correspondence may be addressed: Dept. of Molecular Genetics, University of Texas Southwestern Medical Center, 5323 Harry Hines Blvd., Dallas, TX 75390-9046. Tel.: 214-648-3467; E-mail: Russell.DeBose-Boyd@utsouthwestern.edu.

[2] The abbreviations used are: ER, endoplasmic reticulum; HMGCR, HMG-CoA reductase; ERAD, endoplasmic reticulum-associated degradation; 24,25-DHL, 24,25-dihydrolanosterol; Insig, insulin-induced gene; SREBP, sterol regulatory element-binding protein; HIF, hypoxia-inducible factor; Tg, transgenic; VHL, von Hippel-Lindau; DMOG, dimethyloxalylglycine; RT-PCR, real-time PCR; HRE, hypoxia-responsive element.

isoforms of Insig-2 mRNA, designated Insig-2a and Insig-2b, are expressed in the liver (12, 14). These isoforms are derived from a single Insig-2 gene and encode identical proteins. The nucleotide sequences of Insig-2a and Insig-2b mRNAs differ only in their non-coding first exons; Insig-2a contains exon 1a, whereas Insig-2b contains exon 1b. This difference results from transcription driven by alternative promoters, accounting for the differential regulation of Insig-2a and Insig-2b mRNAs. The Insig-2a mRNA is expressed exclusively in the liver, and its expression is repressed by insulin. The Insig-2b transcript is expressed ubiquitously, and its expression is not regulated by insulin.

The synthesis of one molecule of cholesterol from the precursor acetyl-CoA requires 11 molecules of dioxygen (15, 16) (Fig. 1). One molecule of dioxygen is required for the epoxidation of squalene, which is catalyzed by the enzyme squalene monooxygenase. Nine molecules of dioxygen are utilized by lanosterol 14-$\alpha$ demethylase and C4-methyl sterol oxidase in the successive removal of the 4$\alpha$, 4$\beta$, and 14$\alpha$ methyl groups from lanosterol and 24,25-DHL. Finally, sterol 5-desaturase consumes one molecule of dioxygen in the reduction of lathosterol to 7-dehydrocholesterol. Previously, we found that oxygen deprivation (hypoxia) inhibits cholesterol synthesis and causes lanosterol and 24,25-DHL to accumulate in CHO cells (17). The accumulation of 24,25-DHL serves as one signal for accelerated degradation of HMGCR, which ultimately reduces flux through early steps in cholesterol synthesis when oxygen is limiting. The second signal is provided by the hypoxic induction of Insigs through a reaction that requires the oxygen-sensitive transcription factor hypoxia-inducible factor 1$\alpha$ (HIF-1$\alpha$) (18, 19). This study expands these findings by demonstrating that *Insig-2* is a *bona fide* HIF target gene in cultured human fibroblasts and in livers of mice. Experiments utilizing genetically manipulated mice show that Insig-2-dependent degradation significantly contributes to HIF-mediated regulation of hepatic HMGCR, highlighting the physiologic relevance of the response. Thus, the link between oxygen sensing and feedback regulation of cholesterol synthesis extends beyond cultured cells to whole animals.

## Results

HIF is a heterodimeric transcription factor composed of a labile $\alpha$ subunit and a stable $\beta$ subunit (18, 19). Under normal oxygen conditions, the $\alpha$ subunit is hydroxylated on two proline residues, allowing the protein to become recognized by the von Hippel-Lindau (VHL) tumor suppressor protein for subsequent ubiquitination and proteasomal degradation. Under low-oxygen conditions (hypoxia), the $\alpha$ subunit is not hydroxylated because of the strict requirement for molecular oxygen by prolyl hydroxylases that modify the protein. Stabilized $\alpha$ subunits bind to $\beta$ subunits and activate transcription by binding to HREs present in more than 70 HIF target genes (20). Enhanced expression of HIF target genes, which mediate several cellular processes such as growth and apoptosis, angiogenesis, and energy metabolism, allows for adaptation to hypoxia at the cellular, tissue, and organismal levels. Fig. 2 examines the expression of Insig mRNAs in human SV-589 cells treated with DMOG. This cell-permeable analog of 2-oxoglutarate inhibits

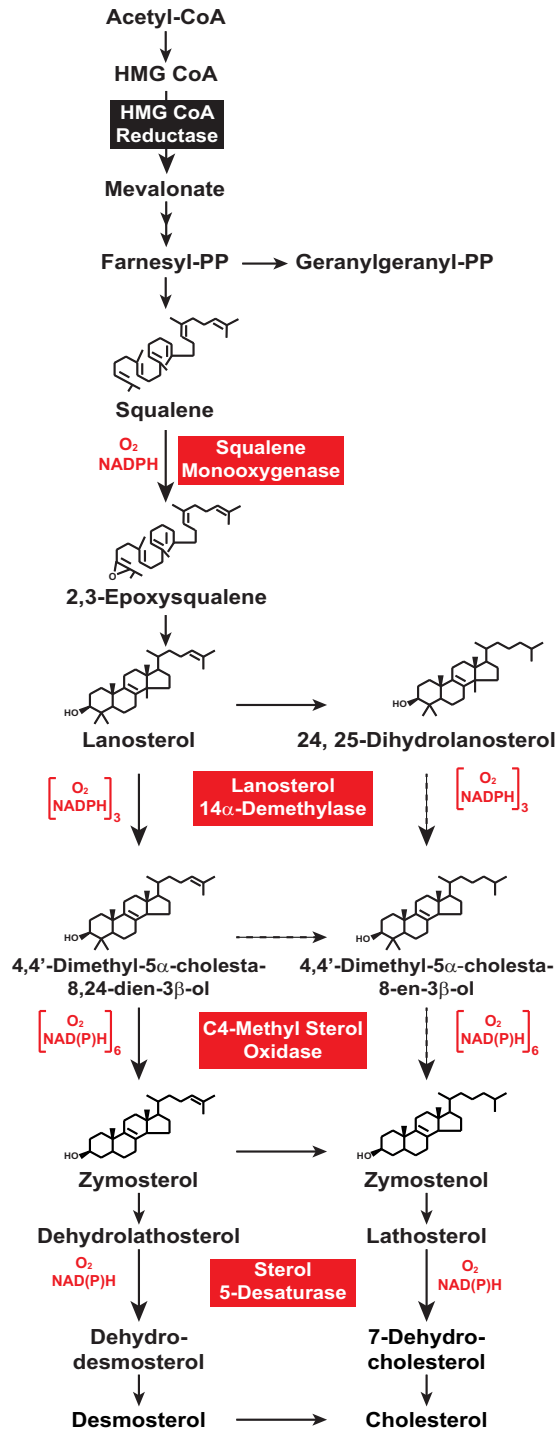


**Figure 1. The cholesterol biosynthetic pathway in animal cells.** The schematic of the cholesterol biosynthetic pathway is based on recent flux studies by Mitsche *et al.* (42). Reactions that require molecular oxygen are highlighted in *red*.

2-oxoglutarate-dependent dioxygenases, including prolyl hydroxylases that modify and destabilize HIF$\alpha$ subunits (21). SV-589 cells were incubated for 24 h with various concentrations of DMOG prior to harvest and subcellular fractionation. Subsequent immunoblot analysis revealed that DMOG caused nuclear accumulation of HIF-1$\alpha$ (Fig. 2*A*, *lanes b–e*) and enhanced expression of the mRNA for VEGF, an established HIF target gene (Fig. 2*B*). DMOG markedly stimulated the

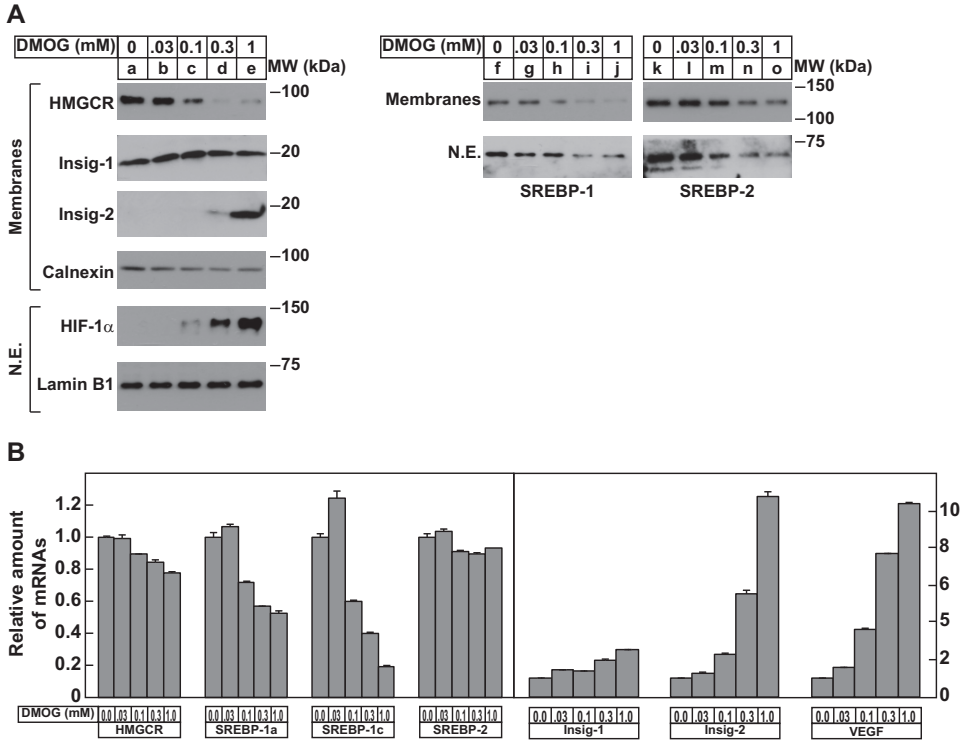


**Figure 2. DMOG enhances expression of Insig-2 and suppresses HMGCR in SV-589 cells.** *A* and *B*, SV-589 cells were set up on day 0 at $6.0 \times 10^5$ cells/100-mm dish in medium A containing 10% FCS. On day 1, cells were switched to the identical medium with the indicated concentration of DMOG. Following incubation for 24 h at 37 °C, cells were harvested for subcellular fractionation (*A*) or isolation of total RNA (*B*) as described under "Experimental Procedures." *A*, resulting membrane and nuclear extract (*N.E.*) fractions were subjected to SDS-PAGE (10–30 $\mu$g of total protein/lane), followed by immunoblot analysis with antibodies against HMGCR, Insig-1, Insig-2, calnexin, HIF-1$\alpha$, Lamin B1, SREBP-1, and SREBP-2. *MW*, molecular weight. *B*, total RNA from each condition was subjected to quantitative RT-PCR using primers against the indicated gene; cyclophilin B mRNA was used as an invariant control. Each value represents the amount of mRNA relative to that in vehicle-treated cells, which is arbitrarily defined as 1. *Error bars* represent ± S.E. of triplicate samples.

expression of Insig-2 protein and mRNA (~10-fold); expression of Insig-1 mRNA was also enhanced by DMOG but to a lesser extent (~2-fold) than that observed for Insig-2 mRNA (Fig. 2*B*). Insig-1 protein remained unchanged in the presence of DMOG (Fig. 2*A*, *lanes b–e*). DMOG-induced expression of Insig-2 mRNA was observed in multiple cell lines from various tissues, including CHO-7, HepG2 (human hepatoma), primary rat hepatocytes, and AML12 (mouse hepatocytes); however, induction of Insig-1 mRNA was limited to CHO-7 cells and primary rat hepatocytes (data not shown). The amount of HMGCR protein in membranes was reduced by DMOG (Fig. 2*A*, *lanes b–e*), which likely resulted from accelerated degradation, as indicated by the slight reduction in the amount of HMGCR mRNA (Fig. 2*B*). Membrane-bound and nuclear forms of SREBPs were modestly reduced by DMOG treatment (Fig. 2*A*, *lanes f–o*), which can be attributed to reduced expression of mRNAs encoding the SREBP-1 isoforms SREBP-1a and SREBP-1c (Fig. 2*B*).

To determine the individual contribution of Insigs to the DMOG-induced degradation of HMGCR, we used the CRISPR/Cas9 system to generate Insig-deficient SV-589 cells. Fig. 3*A* shows that DMOG treatment of parental SV-589 cells stimulated the degradation of HMGCR and accumulation of Insig-2, HIF-1$\alpha$, and HIF-2$\alpha$ as expected (*lanes 1* and *2*). These responses continued in SV-589 cells deficient in Insig-1 (Fig. 3*A*, *lanes 3* and *4*). In contrast, DMOG no longer stimulated degradation of HMGCR in Insig-2-deficient SV-589 cells even though the inhibitor continued to stimulate accumulation of HIF-1$\alpha$ and HIF-2$\alpha$ in the nucleus (Fig. 3*A*, *lanes 5* and *6*).

RNAi was utilized to identify the HIF$\alpha$ subunit required for DMOG-mediated induction of Insig-2 and subsequent degradation of HMGCR. In the experiment shown in Fig. 3*B*, SV-589 cells were transfected with siRNAs against the mRNA encoding the control GFP, HIF-1$\alpha$, or HIF-2$\alpha$; scrambled versions of the HIF-1$\alpha$ and HIF-2$\alpha$ siRNAs were utilized as negative controls. The results show that, in cells transfected with the GFP siRNA, DMOG stabilized HIF-1$\alpha$ and HIF-2$\alpha$, enhanced expression of Insig-2, and stimulated degradation of HMGCR (Fig. 3*B*, *lanes 1* and *2*). RNAi-mediated knockdown of HIF-1$\alpha$ abolished DMOG-mediated induction of Insig-2 and degradation of HMGCR (Fig. 3*B*, *lanes 3* and *4*); however, both reactions continued and were somewhat enhanced in HIF-2$\alpha$ knockdown cells (Fig. 3*B*, *lanes 5* and *6*). DMOG stimulated Insig-2 expression and HMGCR degradation in cells transfected with scrambled HIF-1$\alpha$ and HIF-2$\alpha$ siRNAs (Fig. 3*B*, *lanes 7-10*). Consistent with this, DMOG-induced expression of Insig-2 mRNA was blunted by HIF-1$\alpha$ but not by HIF-2$\alpha$ knockdown (Fig. 3*C*). DMOG continued to enhance the expression of mRNAs encoding VEGF and glucose transporter 1 (GLUT1) in HIF-1$\alpha$ and HIF-2$\alpha$ knockdown cells (Fig. 3*C*), indicating that the two HIF$\alpha$ subunits are interchangeable in the regulation of these genes.

The human *INSIG-2* gene is organized similarly to the mouse gene (Fig. 4*A*). Considering this, we next sought to determine

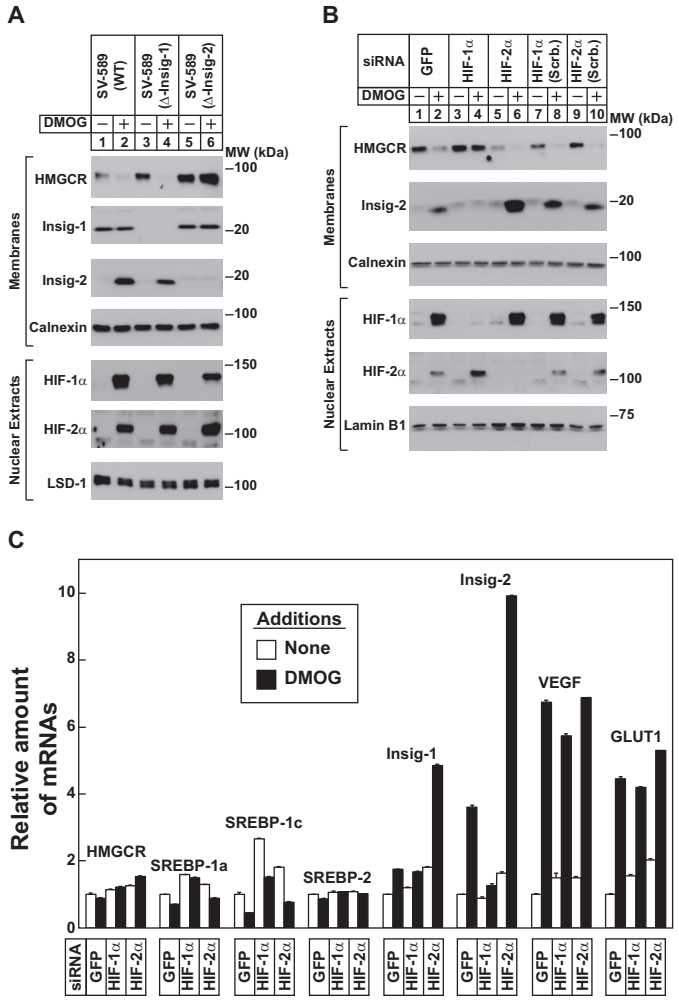


**Figure 3. DMOG suppresses HMGCR in SV-589 cells through a mechanism requiring HIF-1$\alpha$ and Insig-2.** *A*, SV-589 (WT), SV-589 (ΔInsig-1), and SV-589 (ΔInsig-2) cells were set up on day 0 at 6.0 × $10^5$ cells/100-mm dish in medium A containing 10% FCS. On day 1, cells were switched to the identical medium in the absence or presence of 0.3 mM DMOG. Following incubation for 24 h at 37 °C, cells were harvested for subcellular fractionation. The resulting membrane and nuclear extract fractions were subjected to SDS-PAGE (10–30 $\mu$g total protein/lane), followed by immunoblot analysis with antibodies against HMGCR, Insig-1, Insig-2, calnexin, HIF-1$\alpha$, HIF-1$\alpha$, and LSD-1. *MW*, molecular weight. *B* and *C*, SV-589 cells were set up on day 0 at 2.5 × $10^5$ cells/100-mm dish in medium A containing 10% FCS. On day 1, cells were transfected with siRNAs targeting mRNAs encoding GFP, HIF-1$\alpha$, and HIF-2$\alpha$, as indicated and described under "Experimental Procedures." Scrambled (*Scrb.*) HIF-1$\alpha$ and HIF-2$\alpha$siRNAs were used as additional negative controls. On day 2, cells were treated in the absence or presence of 0.3 mM DMOG for 24 h at 37 °C, after which they were harvested for subcellular fractionation (*B*) and total RNA isolation (*C*) as described under "Experimental Procedures." *B*, aliquots of membrane and nuclear extract fractions (10–30 $\mu$g total protein/lane) were subjected to SDS-PAGE, followed by immunoblot analysis with antibodies against HMGCR, Insig-2, calnexin, HIF-1$\alpha$, HIF-2$\alpha$, and Lamin B1. *C*, total RNA from each condition was subjected to quantitative RT-PCR as described in the legend for Fig. 2*B*. *Error bars* denote ± S.E. of triplicate samples.

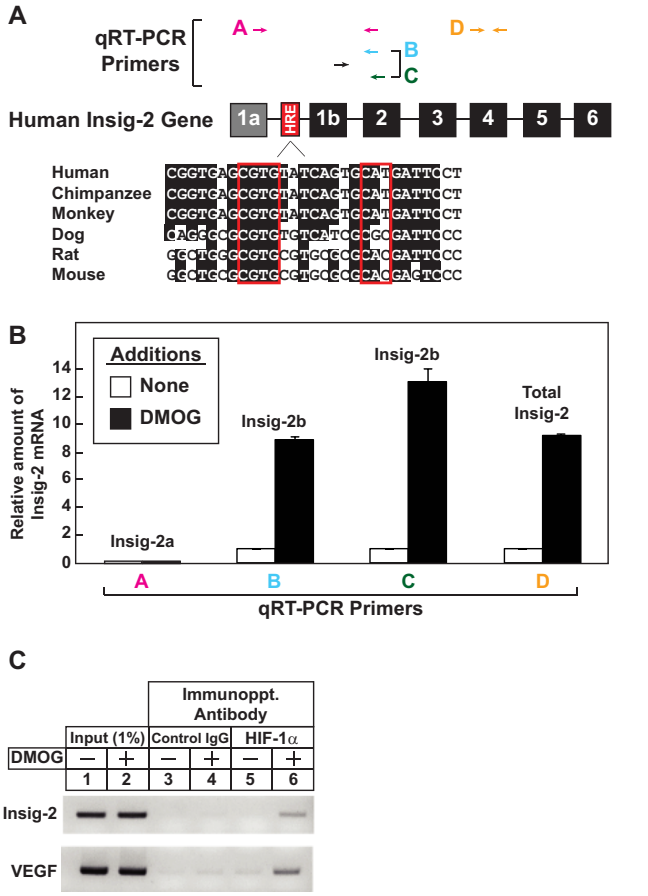


**Figure 4. DMOG enhances binding of HIF-1$\alpha$ to HRE within intron 1 of the human *INSIG-2* gene.** *A*, schematic of the human Insig-2 gene, showing the location of exons and HRE (*top panel*) and conservation of the Insig-2 HRE sequence across species (*bottom panel*). Exons are indicated by *boxes* labeled with the corresponding exon numbers. The position of HRE conserved in mammalian species is indicated by a *red box*. *Arrows* denote the location of the primers used in the quantitative RT-PCR experiment shown in *B*. *B*, total RNA isolated from SV-589 cells treated with or without 1 mM DMOG for 24 h at 37 °C was subjected to quantitative RT-PCR as described in the legend to Fig. 2*B* using primer pairs A–D; cyclophilin B mRNA was used as an invariant control. Each value represents the amount of mRNA relative to that in untreated cells, which is arbitrarily defined as 1. *Error bars* represent the ± S.E. of triplicate samples. *C*, SV-589 cells were set up on day 0 at 1.0 × $10^6$ cells/150-mm dish in medium A containing 10% FCS. On day 1, cells were switched to the identical medium in the absence or presence of 1 mM DMOG. Following incubation for 24 h at 37 °C, cells were fixed with formalin. After the sheared chromatin was incubated with 4 $\mu$g of anti-HIF-1$\alpha$ IgG or control IgG, DNA was purified from each immunoprecipitate and subjected to PCR with primers that flank the HREs in the human Insig-2 or VEGF genes as described under "Experimental Procedures." The resulting PCR products were visualized on an agarose gel by ethidium bromide staining. *Immunoppt.*, immunoprecipitating.

whether the Insig-2a or Insig-2b transcript becomes induced upon treatment of human SV-589 cells with DMOG. The quantitative real-time PCR experiment shown in Fig. 4*B* shows that the Insig-2a transcript was barely detectable in SV-589 cells, and its expression was not enhanced by DMOG treatment (*primer pair A*). However, DMOG-induced expression of the Insig-2b transcript was readily observed in quantitative real-time PCR reactions (Fig. 4*B*, *primer pairs B* and *C*). A similar magnitude of DMOG-induced expression was observed for total Insig-2 mRNA (Fig. 4*B*, *primer pair D*).

Sequence analysis revealed the presence of conserved sequences conforming to the consensus HRE (5′-CGTG$X_{(1-8)}$-CAC/T-3′) within the intronic region between exons 1a and 1b of the human *INSIG-2* gene. In the experiment shown in Fig. 4*C*, we used ChIP assays to determine whether HIF physically interacts with the putative Insig-2 HRE. SV-589 cells were treated in the absence or presence of DMOG for 24 h. Following cross-linking of protein-DNA complexes, samples were immunoprecipitated with either control IgG or anti-HIF-1$\alpha$ IgG. When HIF-1$\alpha$ was immunoprecipitated from

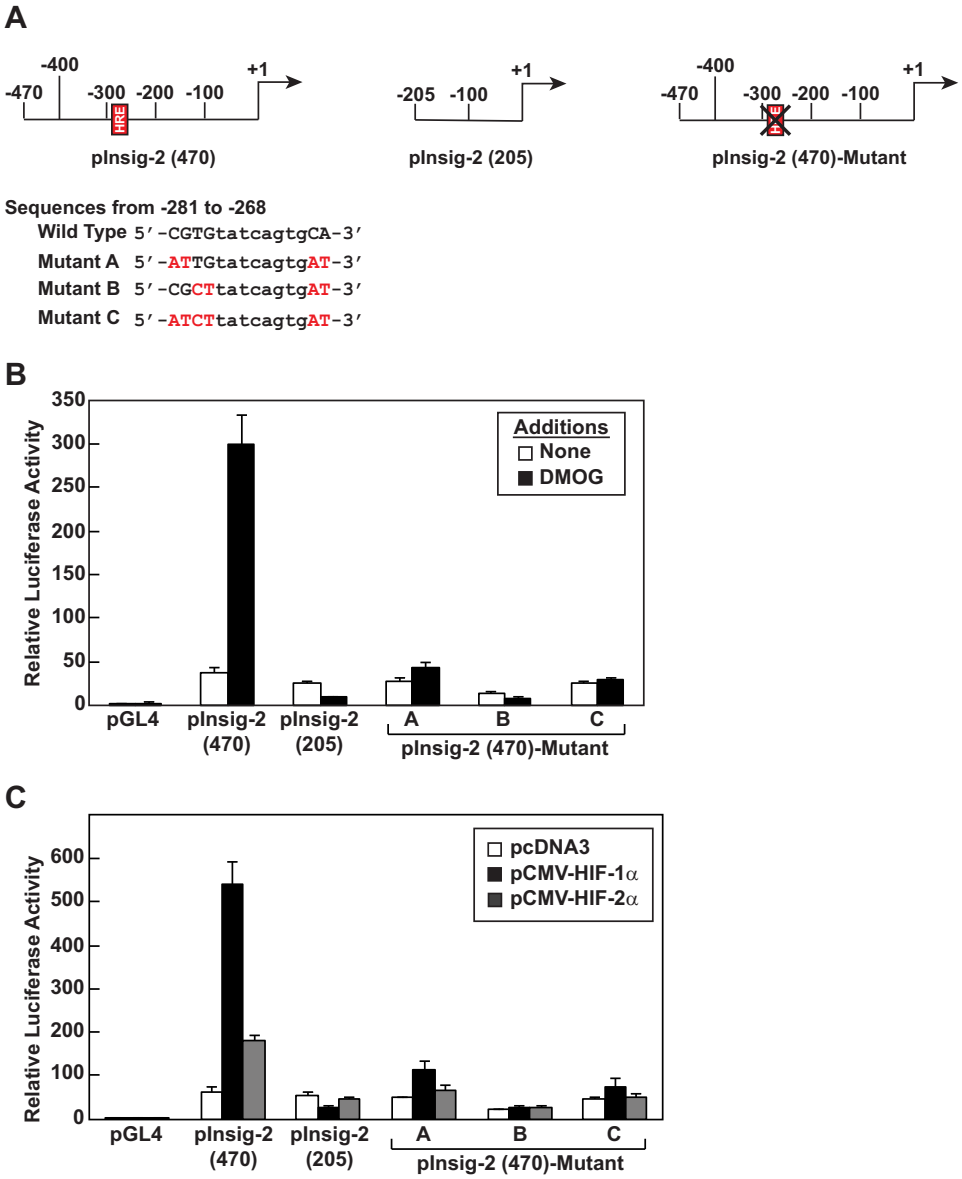


**Figure 5. DMOG treatment and HIF overexpression in SV-589 cells activate the human Insig-2 promoter through an HRE-dependent mechanism.** *A*, schematic of pInsig-2 (470) encoding a fragment of intron 1 of the human Insig-2 gene containing the putative HRE (nucleotides −470 to +1 relative to the start site of transcription of the Insig-2 mRNA) linked to the pGL4 firefly luciferase reporter; pInsig-2 (205) contains the luciferase reporter linked to intronic sequences −205 to +1 (relative to the start site of transcription of the Insig-2 mRNA) of the Insig-2 gene, whereas pInsig-2 (470)-Mutant contains the luciferase reporter linked to the 470-nucleotide intronic fragment harboring various mutations within the putative HRE. The sequence of the wild-type and mutant HRE in the human Insig-2 promoter is shown, with mutated nucleotides highlighted in *red* (*bottom panel*). *B* and *C*, SV-589 cells were set up on day 0 at $4.5 \times 10^4$ cells/well of a 6-well plate in medium A containing 10% FCS. *B*, on day 1, cells were transfected with *Renilla* luciferase and the indicated Insig-2 HRE-luciferase reporter plasmids as described under "Experimental Procedures." Following incubation for 5 h at 37 °C, cells were switched to medium A containing 10% FCS in the absence or presence of 1 mM DMOG. After 24 h at 37 °C, cells were harvested, and luciferase activity was measured. Each value represents the amount of firefly luciferase activity normalized to *Renilla* luciferase activity relative to that in untreated cells transfected with pGL4, which is arbitrarily defined as 1. *Error bars* denote ± S.E. of three independent experiments. *C*, SV-589 cells were set up on day 0 and transfected on day 1 with *Renilla* luciferase and the Insig-2 HRE-luciferase reporter plasmids in the absence or presence of plasmids encoding non-degradable HIF-1α (*pCMV-HIF-1α*) or HIF-2α (*pCMV-HIF-2α*) as described in *B*. On day 2, cells were harvested, and luciferase activity was measured. Values represent firefly luciferase activity normalized to *Renilla* luciferase activity relative to that in mock-transfected cells, which is arbitrarily defined as 1. *Error bars* denote the mean ± S.E. of three independent experiments.

DMOG-treated samples, the Insig-2 HRE was among the HIF-associated DNA fragments, as determined by PCR analysis of precipitated material (Fig. 4*C*, *lane 6*). The Insig-2 HRE failed to be amplified from samples precipitated with control IgG (Fig. 4*C*, *lane 4*). As expected, DNA fragments corresponding to the HRE of the VEGF gene were isolated in anti-HIF-1α immunoprecipitates (Fig. 4*C*, *lane 6*).

To further explore the mechanism of HIF-mediated regulation of Insig-2, a 470-nucleotide fragment between exons 1a and 1b of the human *INSIG-2* gene was inserted upstream of a firefly luciferase reporter gene in the promoterless pGL4 vector (Fig. 5*A*). When the resultant reporter plasmid was introduced into SV-589 cells, luciferase activity was increased ~6-fold upon incubation of the cells with DMOG (Fig. 5*B*). DMOG-mediated induction of luciferase activity was abolished by removal of nucleotides −470 to −206 or by mutation of the HRE sequence (Fig. 5*B*). Fig. 5*C* shows that luciferase activity was stimulated 5- or 2-fold upon co-expression of non-degrad-

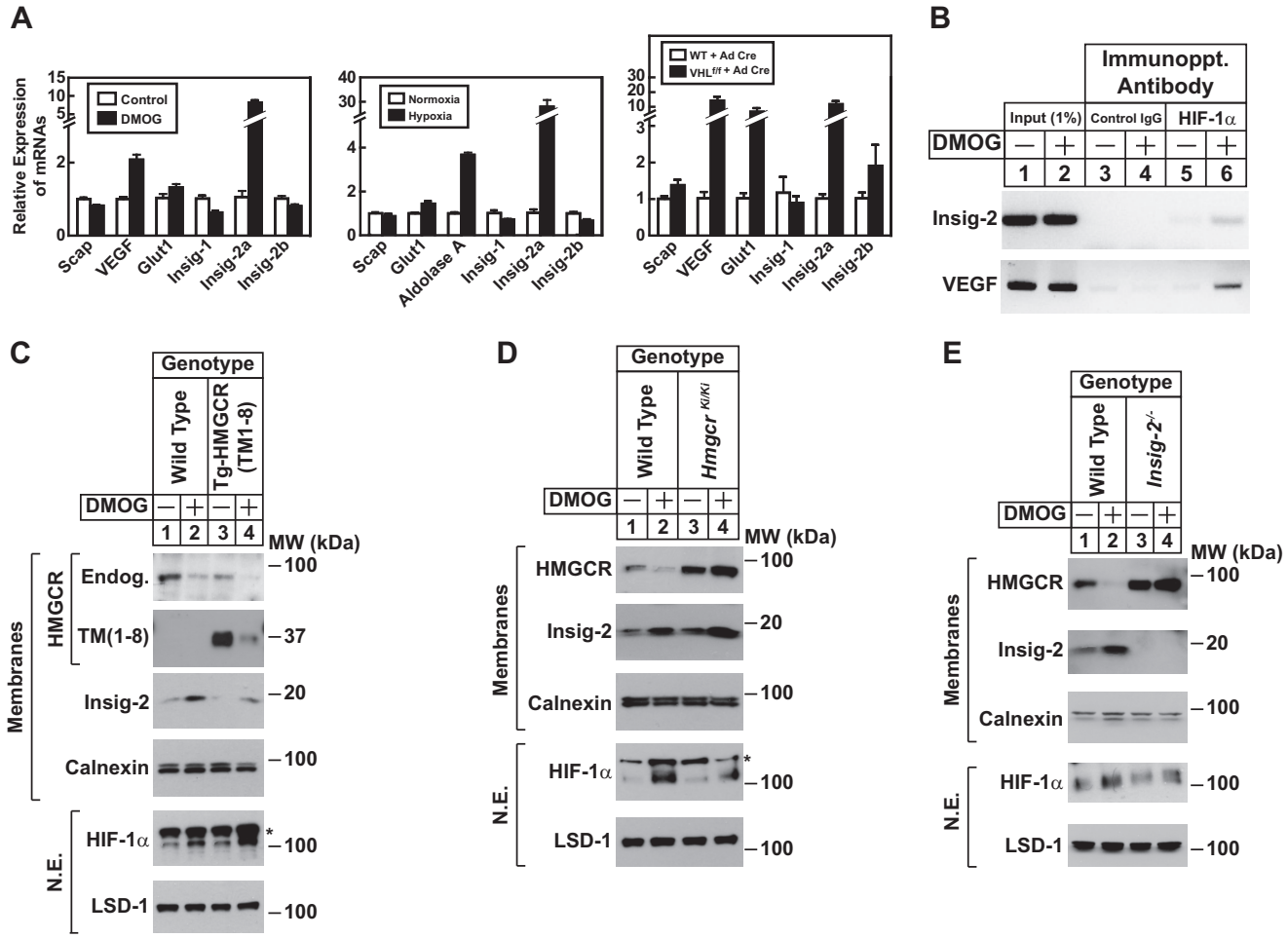


**Figure 6. DMOG-induced expression of the Insig-2a transcript stimulates degradation of HMGCR in livers of mice.** *A*, wild-type C57BL/6J male mice (8–11 weeks of age) were either administered 8 mg/day of DMOG in saline by oral gavage for 5 consecutive days or exposed to normoxia (21% $O_2$) or hypoxia (6% $O_2$) for 6 h as described under "Experimental Procedures." *Vhl*$^{f/f}$ mice and wild-type littermates were injected with an adenovirus encoding for Cre recombinase driven by the CMV promoter. Mice were analyzed 4 days after injection. At the end of the treatment periods, the mice were sacrificed. RNA was isolated from the liver, and quantitative real-time PCR analysis was performed as described in the legend for Fig. 2. Each value represents the expression of the indicated gene relative to that in the control group. Data are presented as means ± S.E. ($n = 3$ for each group subjected to DMOG and hypoxia treatment; $n = 6$ for each group injected with adenovirus encoding Cre recombinase). *B*, ChIP assays were performed with livers from male C57BL/6J mice administered intraperitoneal DMOG (8 mg) or saline once daily for 3 days. Four hours after the final injection, liver tissues were fixed with formalin and subjected to ChIP assays using primers that flank HRE in the mouse Insig-2 or VEGF genes as described under "Experimental Procedures." *Immunoppt.*, immunoprecipitating. *C–E*, male mice (8–11 weeks of age, 4–6 mice/group) of the indicated genotypes were injected intraperitoneally with DMOG (8 mg) or saline once daily for 3 days. Mice were sacrificed 6 h following the third injection, and livers were harvested for subcellular fractionation as described under "Experimental Procedures." Aliquots of membrane and nuclear extract (*N.E.*) fractions (20–50 μg of total protein/lane) for each group were pooled and subjected to immunoblot analysis using anti-T7 IgG (against HMGCR (TM1–8)) and antibodies against endogenous (*Endog.*) HMGCR, Insig-2, calnexin, HIF-1α, and LSD-1. The *asterisks* in the HIF-1α blot denote a cross-reactive nonspecific band. *MW*, molecular weight.

able HIF-1α or HIF-2α, respectively, with the full-length, wild-type reporter plasmid. HIF-mediated induction of luciferase activity was abolished by truncation of the Insig-2 fragment or by mutation of the HRE. Nearly identical results were obtained with human Huh 7 cells (supplemental Fig. 1).

Expression of Insig-2 was next examined in livers of mice in which HIF levels were modulated by pharmacologic prolyl hydroxylase inhibition, oxygen deprivation, or genetic manipulation. Administration of DMOG to mice by oral gavage (8 mg/day for 5 consecutive days) resulted in a marked increase in the expression of hepatic Insig-2a mRNA (Fig. 6*A*). The levels of Insig-1 and Insig-2b mRNAs were not increased, whereas the mRNAs for GLUT1 and VEGF were elevated in the livers of DMOG-treated mice as expected.

In the oxygen deprivation model, mice were exposed to hypoxia (6% $O_2$) for 6 h. Control mice were maintained at normoxia (21% $O_2$) in the same room. Food was withdrawn from both groups during the treatment period to control for any effects of insulin. Fig. 6*A* shows that hypoxia led to a 28-fold increase in the amount of Insig-2a mRNA in the mouse liver. Consistent with changes in DMOG-treated mice, we observed a slight decrease in the amount of Insig-1 and Insig-2b mRNA in the hypoxic mouse livers. Expression of mRNAs for the HIF targets GLUT1 and aldolase A was elevated by hypoxia as expected.

We next examined mice that harbored a floxed *Vhl* allele (*Vhl*$^{f/f}$) (22). *Vhl*$^{f/f}$ and control wild-type mice were injected with an adenovirus encoding for Cre recombinase driven by the cytomegalovirus promoter. Because von Hippel-Lindau tumor suppressor protein is required for oxygen-dependent degradation of HIFα subunits, recombination of the *Vhl* allele results in constitutive HIF activation. Four days after injection, expres-

sion of the HIF target genes VEGF and GLUT1 was found to be increased in the livers of *Vhl* knock-out mice, indicating successful recombination in the liver (Fig. 6*A*). Hepatic Insig-2a mRNA was increased 12-fold in *Vhl* knock-out mice compared with their wild-type counterparts. The levels of Insig-1 and Insig-2b mRNA were not different between *Vhl* knock-out and wild-type mice.

Sequence analysis of the mouse *Insig-2* gene, including ~8 kb upstream of the transcriptional start site of exon 1b, revealed the presence of three putative HRE sequences (supplemental Fig. 2*A*). Thus, a series of reporter plasmids were generated in the pGL4 vector that contained different portions of the mouse Insig-2 5′-flanking region and the first intron fused to firefly luciferase. These plasmids were then co-expressed in primary rat hepatocytes, which mimic the liver in expression of Insig-2a and Insig-2b (14), together with non-degradable HIF-1$\alpha$ to identify a functional HRE. Luciferase activity was not stimulated when non-degradable HIF-1$\alpha$ was co-expressed with empty pGL4 vector or the reporter plasmid containing the 3.64-kb region directly upstream of exon 1a of the *Insig-2* gene (supplemental Fig. 2*B*). In contrast, HIF-1$\alpha$ expression led to a marked induction of luciferase activity in hepatocytes transfected with the reporter plasmid containing nucleotides that span the intronic region between exons 1a and 1b (supplemental Fig. 2*B*). Analyses of truncation mutants traced this HIF-mediated induction to a region ~440 nucleotides upstream of exon 1b of the mouse *Insig-2* gene.

Two sequences that conform to the consensus HRE are present in the 440-nucleotide region upstream exon 1b of the *Insig-2* gene. We designated the more distal sequence candidate HRE-1 and the more proximal sequence candidate HRE-2. The experiment shown in supplemental Fig. 2*C* evaluated HIF-dependent regulation of the truncated pGL4 reporter plasmid harboring mutations in HRE-1 or HRE-2. HIF-mediated induction of luciferase activity was observed with the reporter plasmid containing the wild-type upstream sequence, as expected. Similar results were observed with the plasmid harboring mutations in the candidate HRE-2 sequence. However, HIF-mediated induction of luciferase activity was abolished by mutation of the HRE-1 sequence. A direct role for HIF-1$\alpha$ in the regulation of hepatic Insig-2 is indicated by the ChIP experiment shown in Fig. 6*B*, which shows that, in livers of mice, DMOG treatment stimulated binding of HIF-1$\alpha$ to HREs present in the first intron of the *Insig-2* gene and the VEGF promoter.

Studies were next carried out to determine whether DMOG-induced expression of Insig-2 modulates degradation of HMGCR. For this purpose, we utilized a recently developed line of transgenic mice, designated Tg-HMGCR (TM1–8) (23), expressing in the liver the membrane domain of HMGCR that is both necessary and sufficient for Insig-mediated, sterol-accelerated degradation (3). Fig. 6*C* shows that administration of DMOG caused an increase of Insig-2 protein and a reduction of endogenous HMGCR protein in membranes from wild-type (*lane 2*) and Tg-HMGCR (TM1–8) mice (*lane 4*). This was accompanied by enhanced expression of the Insig-2a mRNA and reduced expression of HMGCR mRNA (Fig. 7*A*). DMOG also caused a reduction of HMGCR (TM1–8) protein in livers of transgenic mice (Fig. 6*C*, *lane 4*); however, the compound failed to inhibit expression of HMGCR (TM1–8) mRNA (Fig. 7*A*). DMOG stabilized HIF-1$\alpha$ in the nucleus (Fig. 6*C*, *lane 4*) and enhanced expression of the HIF-target genes VEGF and GLUT1 (Fig. 7*A*) in wild-type and transgenic mouse livers as expected.

In addition to Tg-HMGCR (TM1–8) mice, we developed a line of knockin mice, designated $Hmgcr^{Ki/Ki}$, to determine the contribution of accelerated degradation to the overall regulation of HMGCR in the liver (23). $Hmgcr^{Ki/Ki}$ mice harbor mutations in the endogenous HMGCR gene that abolish sterol-induced ubiquitination and degradation of HMGCR protein (2). Administration of DMOG stabilized HIF-1$\alpha$ and enhanced expression of Insig-2 protein and mRNA in the livers of both wild-type and $Hmgcr^{Ki/Ki}$ mice (Figs. 6*D*, *lanes 2* and *4*, and 7*B*). DMOG reduced HMGCR protein in the livers of wild-type mice (Fig. 6*D*, *lane 2*); however, the protein remained constant in $Hmgcr^{Ki/Ki}$ livers (Fig. 6*D*, *lane 4*) even though the expression of HMGCR mRNA in the livers of both was inhibited by DMOG treatment (Fig. 7*B*). Importantly, DMOG also failed to enhance degradation of HMGCR in the livers of Insig-2 knock-out mice (designated $Insig\text{-}2^{-/-}$) even though the compound stabilized HIF-1$\alpha$ (Fig. 6*E*, *lane 4*).

## Discussion

Our data provide further insights into the molecular mechanisms that link oxygen sensing and the pathway for HMGCR ERAD. This link is illustrated when human SV-589 cells are treated with the prolyl hydroxylase inhibitor DMOG, which mimics hypoxia by stabilizing the oxygen-sensitive transcription factor HIF-1$\alpha$. The treatment stimulated degradation of HMGCR (Fig. 2) via a reaction that required the presence of Insig-2 and HIF-1$\alpha$ (Fig. 3, *A* and *B*). These results led to the identification of a functional HRE within the intronic region between exon 1a and exon 1b of the human *INSIG-2* gene (Figs. 4, *A* and *B*, and 5) that bound HIF-1$\alpha$ (Fig. 4*C*). Considered together, these observations are consistent with the scenario depicted in Fig. 7*D*, which shows that HIF-1$\alpha$ becomes stabilized upon prolyl hydroxylase inhibition and subsequently binds to HRE sequences within the promoter of the *INSIG-2* gene to activate transcription. This activation leads to enhanced expression of Insig-2 mRNA and accumulation of Insig-2 protein. Accumulated Insig-2 protein then binds to HMGCR, triggering its accelerated ubiquitination and degradation.

The physiologic relevance of HIF-mediated regulation of Insig-2 was indicated by hepatic induction of the transcript in three mouse models of actual or approximated hypoxia: oxygen deprivation, pharmacologic prolyl hydroxylase inhibition, and VHL knockout (Fig. 6*A*). DMOG stimulated the degradation of the membrane domain of HMGCR that was expressed under liver-specific, sterol-independent transcriptional control (Fig. 6*C*). In contrast, HMGCR harboring mutations that prevent sterol-induced ubiquitination resisted DMOG-induced degradation in the liver (Fig. 6*D*). Finally, HMGCR failed to become degraded in the livers of Insig-2-deficient mice subjected to DMOG treatment (Fig. 6*E*). DMOG is a nonspecific prolyl hydroxylase inhibitor; however, resistance of HMGCR to

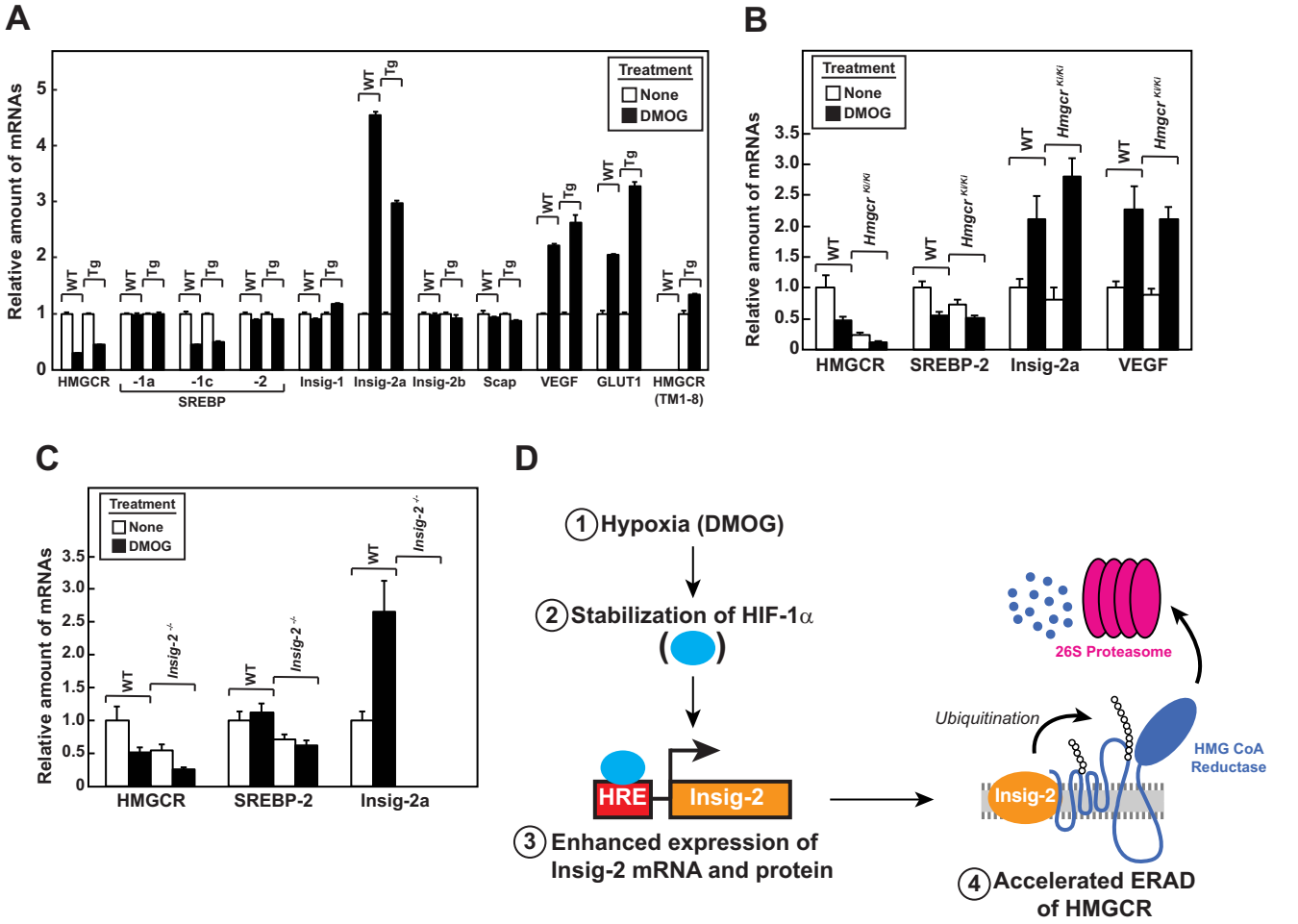


**Figure 7. DMOG modulates the expression of mRNAs encoding components of the Scap-SREBP pathway in livers of mice.** *A–C*, control and Tg-HMGCR (TM1–8) (*A*), $Hmgcr^{Ki/Ki}$ (*B*), or $Insig\text{-}2^{-/-}$ (*C*) mice (the same as used for Fig. 6, *C–E*) were administered intraperitoneal saline in the absence or presence of DMOG (8 mg) once daily for 3 days. Mice were sacrificed 6 h after the third injection, and livers were harvested for total RNA isolation. *A*, total RNA from each tissue was subjected to quantitative PCR using primers for the indicated mRNAs; apoB mRNA was used as an invariant control. Each value represents the amount of mRNA relative to that in the wild type administered saline, which is arbitrarily defined as 1. *Error bars* show the mean ± S.E. of triplicate samples. *B* and *C*, equal amounts of RNA from individual mice were subjected to quantitative RT-PCR using primers against the indicated gene; apoB mRNA was used as an invariant control. Each value represents the amount of mRNA relative to that in the wild type administered saline, which is arbitrarily defined as 1. *Error bars* denote ± S.E. of four to six individual mice. *D*, proposed model for HIF-mediated regulation of HMGCR degradation.

DMOG-induced degradation in $Hmgcr^{Ki/Ki}$ and $Insig\text{-}2^{-/-}$ mice indicates that the reaction occurs through an HIF-mediated mechanism similar to that characterized in cultured cells.

The mouse Insig-2 HRE identified in this study is located ~4500 nucleotides downstream of exon 1a and 285 nucleotides upstream of exon 1b (supplemental Fig. 2*A*). Despite the close proximity of the HRE to exon 1b, HIF modulates expression of Insig-2a but not Insig-2b in mouse livers (Fig. 6*A*) and primary rat hepatocytes (supplemental Fig. 2*B*). This discrepancy can be explained by the fact that transcription factors can modulate gene transcription from distal sites. The classic HIF target gene Epo contains a functional HRE in its 3′ untranslated region (24, 25). The human *INSIG-2* gene is organized similarly to that of the mouse *Insig-2* gene (26). However, the Insig-2b mRNA is regulated by HIF-1α in human SV-589 cells, a fibroblast cell line that does not express Insig-2a (Fig. 4*B*). Similarly, HIF-mediated regulation of Insig-2 mRNA was observed in CHO-7 cells (data not shown), a non-hepatic cell line that does not express Insig-2a. Thus, it appears that HIF mediates the regulation of Insig-2b transcription in the absence of Insig-2a. The molecular basis for this observation merits further investigation.

In the setting of hypoxia, the accumulation of 24,25-DHL coupled with HIF-1α-mediated induction of Insig-2 first triggers degradation of HMGCR, which limits flux through early steps in the cholesterol synthetic pathway (Fig. 1). HIF-2α may also contribute to hypoxia-induced degradation of HMGCR by repressing expression of the *CYP51* gene, which encodes lanosterol 14α-demethylase (27). Upon prolonged hypoxia, processing of SREBPs becomes inhibited because of accumulation of Insig-2, which sensitizes the reaction to sterols. This is consistent with a previous report in which down-regulation of SREBP target genes, including HMGCR, Insig-1, and HMG-CoA synthase, was observed in livers of hypoxic mice (28). Together, these regulatory mechanisms guard against wasting of oxygen and inappropriate cell growth in the face of hypoxic stress. An interesting avenue for future studies will be to examine the role of the cholesterol biosynthetic pathway in other processes modulated by HIF, including angiogenesis and eryth-

ropoiesis. Most renal carcinomas exhibit a clear-cell phenotype and are designated clear-cell renal cell carcinomas (29). The clear-cell phenotype, which results from the abnormal accumulation of neutral lipids, such as triglycerides and cholesterol esters (30, 31), is associated with genetic mutation or silencing of VHL and enhanced stability of HIF-1$\alpha$ and/or HIF-2$\alpha$ (32). Considering the data that link dysregulation of cholesterol metabolism and malignant transformation (33), another exciting line of investigation will be to determine the significance of HIF-mediated regulation of HMGCR degradation in clear-cell renal cell carcinoma development.

## Experimental procedures

### *Cell culture*

Monolayers of SV-589 cells, a line of immortalized human fibroblasts expressing the SV40 large T-antigen (34), were maintained in medium A (DMEM containing 1000 mg/liter glucose, 100 units/ml penicillin, and 100 $\mu$g/ml streptomycin sulfate) supplemented with 10% (v/v) FCS at 37 °C and 5% $CO_2$.

### *RNA interference*

RNA interference was carried out as described previously with minor modifications (9). Duplexes of siRNAs were designed and synthesized by GE Dharmacon (Lafayette, CO). The sequences of the siRNAs used in this study are described in supplemental Table 1. SV-589 cells were set up for experiments on day 0 as described in the figure legends. On day 1, triplicate dishes of cells were incubated with 400 pmol of siRNA duplexes mixed with Lipofectamine RNAiMAX$^{TM}$ reagent (Invitrogen) diluted in Opti-MEM I reduced serum medium (Life Technologies) according to the manufacturer's procedure. Following incubation for 5 h at 37 °C, the cells received a direct addition of medium A containing 10% FCS (final concentration). On day 2, the cells were treated with dimethyloxalylglycine (DMOG). Following incubation for 24 h, the cells were harvested and analyzed as described in the figure legends.

### *Generation of SV-589 cells lacking Insig-1 or Insig-2 using CRISPR/Cas9*

A single guide RNA (GCGCACAGCGCGAGGCGCCG) targeting nucleotides 40–59 (relative to the first initiating methionine) of Insig-1 was cloned into the pSpCas9(BB)-PX330 vector (Addgene, Cambridge, MA). Two single guide RNAs targeting nucleotides −72 to −53 (GACAGTTGAGCTTTTCAGCT) and 194–213 (GCATCTTTTCTTCTGCA) of Insig-2 were cloned into the pSpCas9(BB)-2A-Puro-PX459 vector (Addgene), which harbors the puromycin resistance gene. SV-589 (ΔInsig-1) and (ΔInsig-2) cells were generated as follows. On day 0, SV-589 cells were set up at $4 \times 10^5$ cells/100-mm dish in medium A containing 10% FCS. On day 1, cells were transfected with 1 $\mu$g/dish pSpCas9(BB)-PX330/Insig-1(40–59) together with 3 $\mu$g/dish pcDNA3.1(+) (Thermo Fisher Scientific, Waltham, MA), which harbors the neomycin resistance gene, or 1 $\mu$g/dish pSpCas9(BB)-S2-Puro-PX459/Insig-2 (−72 to −53) and 1 $\mu$g/dish of pSpCas9(BB)-S2-Puro-PX459/Insig-2 (194–213) using FuGENE6 transfection reagent as described previously (3, 8). On day 2, cells were switched to medium A supplemented with 10% FCS and either 700 $\mu$g/ml G418 or 0.5 $\mu$g/ml puromycin to select for SV-589 (ΔInsig-1) and SV-589 (ΔInsig-2) cells, respectively. Fresh medium was added every 2–3 days until colonies formed after 2 weeks. Individual colonies were isolated using cloning cylinders, and the absence of Insig-1 and Insig-2 was determined by immunoblot analysis with rabbit polyclonal anti-Insig-1 antiserum and rabbit polyclonal IgG-940C against human Insig-2. Clones from single colonies of SV-589 (ΔInsig-1) and (ΔInsig-2) cells were isolated by serial dilution in 96-well plates and screened by immunoblot analysis with anti-Insig-1 antiserum and IgG-940C. Sequencing of products obtained from PCR of genomic DNA revealed that SV-589 (ΔInsig-1) cells harbor a 684-bp deletion that encompasses exon 2 encoding the initiating methionine of Insig-1 and a portion of intron 2; SV-589 (ΔInsig-2) cells harbor a 265-bp deletion that removes the initiating methionine and 69 additional amino acids. Monolayers of SV-589 (ΔInsig-1) and (ΔInsig-2) cells were maintained in medium A containing 10% FCS and 700 $\mu$g/ml G418 (ΔInsig-1) or 0.5 $\mu$g/ml puromycin (ΔInsig-2) at 37 °C, 5% $CO_2$.

### *Quantitative real-time PCR*

The protocol for quantitative RT-PCR was similar to that described previously (35). Total RNA was prepared from cultured cells or mouse livers using the RNA STAT-60 kit (TEL-TEST "B", Friendswood, TX) or the RNeasy kit (Qiagen, Hilden, Germany). Equal amounts of RNA were treated with DNase I (DNA-free$^{TM}$, Thermo Fisher Scientific). First-strand cDNA was synthesized from 2 $\mu$g of DNase I-treated total RNA with random hexamer primers using TaqMan reverse transcription reagents (Applied Biosystems/Roche Applied Science, Foster City, CA). Specific primers for each gene were designed using Primer Express software (Life Technologies). Triplicate RT-PCR reactions were set up in a final volume of 20 $\mu$l containing 20 ng of reverse-transcribed total RNA, 167 nM forward and reverse primers, and 10 $\mu$l of 2× SYBR Green PCR Master Mix (Life Technologies). The relative amount of all mRNAs was calculated using the comparative threshold cycle ($C_T$) method. Human cyclophilin B and mouse apoB mRNA were used as the invariant controls for RNA samples prepared from cultured human cells and mouse tissues, respectively. The sequences of the primers for RT-PCR used in this study are listed in supplemental Table 2. Other primers for RT-PCR were described previously (36).

### *Subcellular fractionation and immunoblot analysis*

Subcellular fractionation of cells and mouse livers by differential centrifugation was performed as described previously (23, 37). Aliquots of the resulting membrane and nuclear extract fractions were subjected to SDS-PAGE and immunoblot analysis. The primary antibodies used for immunoblotting to detect SREBP-1 (rabbit polyclonal IgG-211C), SREBP-2 (rabbit monoclonal IgG-22D5), Insig-1 (rabbit polyclonal anti-Insig-1 antiserum), Insig-2 (rabbit polyclonal IgG-940C), and HMGCR (mouse monoclonal IgG-A9 and rabbit polyclonal IgG-839C) were described previously (8, 36, 38, 39). Mouse monoclonal anti-T7 IgG was obtained from EMD Biosciences (San Diego, CA). Rabbit polyclonal anti-calnexin IgG and anti-

HIF-2α IgG were from Novus Biologicals (Littleton, CO), rabbit polyclonal anti-LSD1 IgG was from Cell Signaling Technology (Beverly, MA), rabbit polyclonal anti-lamin B1 IgG was from Abcam (Cambridge, MA), and rabbit polyclonal anti-HIF-1α IgG was from Bethyl Laboratories (Montgomery, TX). Bound antibodies were visualized with peroxidase-conjugated, affinity-purified donkey anti-mouse or anti-rabbit IgG (Jackson ImmunoResearch Laboratories, West Grove, PA) using the SuperSignal CL-HRP substrate system (Thermo Fisher Scientific) according to the manufacturer's instructions. Gels were calibrated with prestained molecular mass markers (Bio-Rad). Filters were exposed to film at room temperature.

### *Chromatin immunoprecipitation analysis*

ChIP analysis was carried out using the EZ-ChIP kit (EMD Millipore, Billerica, MA) according to the manufacturer's instructions. For ChIP analysis of cultured cells, chromatin was cross-linked for 10 min at room temperature by adding formaldehyde to the culture medium of cells at a final concentration of 1% (w/v). After quenching the cross-linking reaction with 125 mM glycine, cells were washed with PBS, scraped, and centrifuged at 700 × *g* at 4 °C for 5 min. Pellets were resuspended in 1 ml of a detergent-containing buffer with protease inhibitors, subjected to sonication on ice for 10-s intervals eight times at 30% maximum power, and subsequently precleared with protein G-agarose beads for 1 h at 4 °C. Precleared lysates were then incubated with 4 μg of preimmune rabbit IgG (negative control) or rabbit polyclonal anti-HIF-1α for 16 h at 4 °C, after which the mixture was incubated with protein G-agarose beads for 1 h at 4 °C. For ChIP analysis of mouse liver, frozen liver tissues were thawed on ice, chopped in PBS, and incubated with formaldehyde at a final concentration of 1% (w/v). The tissues (60 mg) were subjected to sonication on ice for 10-s intervals eight times at 30% maximum power and precleared with protein G-agarose beads for 1 h. Precleared lysates were incubated with 5 μg of preimmune rabbit IgG (negative control) or rabbit polyclonal anti-HIF-1α for 16 h at 4 °C, after which the mixture was incubated with protein G-agarose beads for 1 h at 4 °C.

### *Precipitated protein*

DNA complexes from lysates of cells and mouse tissues were washed and eluted with buffers provided by the manufacturer. The purified DNA was subjected to PCR using the AccuPrime Pfx Supermix kit (Thermo Fisher Scientific); ethidium bromide-stained PCR products were visualized following electrophoresis on 1.5% agarose gels. The primers used in the PCR reactions are described in supplemental Table 3.

### *Expression plasmids*

Sequences containing the 5′-flanking region of the human INSIG-2 gene were amplified by PCR with the Phusion DNA polymerase kit (New England Biolabs, Ipswich, MA) using the genomic DNA isolated from SV-589 cells as a template. The primers used for these amplification reactions are described in supplemental Table 4. The resulting PCR products were gel-purified, subjected to restriction digestion, and subcloned into the multiple cloning site of the promoterless pGL4 vector (Promega, pGL4.10) upstream of a synthetic luciferase coding sequence; this plasmid was designated pInsig-2 (470). Site-directed mutagenesis of the candidate hypoxia-responsive elements (HREs) was performed using the QuikChange XL kit (Stratagene, San Diego, CA) using pInsig-2 (470) as a template and the primers described in supplemental Table 4. The pGL4-TK-*Renilla* luciferase vector, in which *Renilla* luciferase is constitutively expressed under the control of the thymidine kinase (TK) promoter, was obtained from Promega (pGL4.74). The expression plasmids pCMV-HIF-1α and pCMV-HIF-2α encode human HIF-1α and HIF-2α, respectively, harboring alanine substitutions for two proline residues (402 and 564 in HIF-1α and 431 and 531 in HIF-2α) that abolish oxygen-dependent hydroxylation and subsequent proteasomal degradation (40, 41). These plasmids were generated by subcloning the mutant HIF-1α and HIF-2α cDNAs (provided by Drs. Elhadji M. Dioum and Joseph A. Garcia, University of Texas Southwestern Medical Center) into the pcDNA3.1 vector (Invitrogen) under transcriptional control of the CMV promoter. The integrity of each plasmid was confirmed by DNA sequencing.

### *Luciferase assay*

SV-589 cells were transfected with FuGENE6 transfection reagent as described previously (3, 8). The conditions of subsequent incubations are described in the figure legends. Following treatments, cell monolayers were washed with PBS and lysed in 0.4 ml of passive lysis buffer (Promega, Madison, WI) by shaking for 30 min at room temperature. The resulting lysates were then transferred to microcentrifuge tubes and briefly centrifuged to remove insoluble debris. Firefly and *Renilla* luciferase activities were measured in 96-well plates by mixing 20 μl of cleared lysates with the Dual-Luciferase reporter assay system (Promega). The amount of firefly luciferase activity of the transfected cells was normalized to *Renilla* luciferase and expressed relative to the value of the control as indicated in the figure legends.

### *Animal studies*

The previously described Tg-HMGCR (TM1–8) mice are a line of transgenic mice that express in the liver transmembrane domains 1–8 (amino acids 1–346) of hamster HMGCR, followed by three tandem copies of the T7 epitope tag (23). $Hmgcr^{Ki/Ki}$ mice harbor homozygous knockin mutations in which lysine residues 89 and 248 are replaced with arginines; these mutations prevent Insig-mediated ubiquitination and degradation of HMGCR in the liver and other tissues of the knockin mice (23). Insig-$2^{-/-}$ mice are homozygous for a null allele of the Insig-2 gene (36). $Vhl^{f/f}$ mice carry a conditional Vhl-null allele and have been described previously (22). $Vhl^{f/f}$ mice and age-matched wild-type control mice were injected with an adenovirus encoding for Cre recombinase driven by the CMV promoter to achieve liver-specific recombination. Mice were analyzed 4 days after injection.

DMOG dissolved in saline was administered to Tg-HMGCR (TM1–8), $Hmgcr^{Ki/Ki}$ and Insig-$2^{-/-}$ mice by intraperitoneal injection at a dose of 8 mg/day for 3 (Fig. 6, *B–E*) or 5 (Fig. 6*A*) consecutive days. Control mice received saline vehicle. At the end of these treatment periods, mice were sacrificed; the livers were removed, snap-frozen, and stored in liquid $N_2$ until anal-

ysis. Animal procedures involving hypoxia treatment of wild-type and $Vhl^{f/f}$ mice were performed in the Brugarolas laboratory. For the hypoxia treatments, mice were placed in a hypoxic chamber that was equilibrated to atmospheric conditions. Over a 40-min period, the oxygen level was decreased in a stepwise manner to 6% $O_2$ by displacement with $N_2$. Mice were subsequently maintained at 6% $O_2$ for 6 h. Control mice were kept under normal atmospheric conditions within the same room. Food was withdrawn from both groups during the treatment period to control for any effect of nutritional status on Insig-2a expression. All mice were housed in colony cages with a 12-h light/12-h dark cycle and fed *ad libitum* Teklad Mouse/Rat Diet 2016 (Harlan Teklad, Madison, WI). Animal experiments were performed with approval of the Institutional Animal Care and Research Advisory Committee at University of Texas Southwestern Medical Center.

*Author contributions*—S. H. designed the research, analyzed data, performed experiments, and drafted the manuscript. A. D. N., Y. J., L. J. E., and J. B. designed the research, analyzed data, and performed experiments. R. A. D. B. designed the research, analyzed data, and drafted the manuscript.

*Acknowledgments—We thank Kristi Garland-Brasher and Gennipher Young-Smith for technical assistance; Lisa Beatty, Shomanike Head, and Ijeoma Onweneme for help with tissue culture; and Dr. Guosheng Liang for insightful advice.*

## References


1. Goldstein, J. L., DeBose-Boyd, R. A., and Brown, M. S. (2006) Protein sensors for membrane sterols. *Cell* **124,** 35–46
2. Sever, N., Song, B. L., Yabe, D., Goldstein, J. L., Brown, M. S., and DeBose-Boyd, R. A. (2003) Insig-dependent ubiquitination and degradation of mammalian 3-hydroxy-3-methylglutaryl-CoA reductase stimulated by sterols and geranylgeraniol. *J. Biol. Chem.* **278,** 52479–52490
3. Sever, N., Yang, T., Brown, M. S., Goldstein, J. L., and DeBose-Boyd, R. A. (2003) Accelerated degradation of HMG CoA reductase mediated by binding of insig-1 to its sterol-sensing domain. *Mol. Cell* **11,** 25–33
4. Song, B. L., Javitt, N. B., and DeBose-Boyd, R. A. (2005) Insig-mediated degradation of HMG CoA reductase stimulated by lanosterol, an intermediate in the synthesis of cholesterol. *Cell Metab.* **1,** 179–189
5. Nguyen, A. D., Lee, S. H., and DeBose-Boyd, R. A. (2009) Insig-mediated, sterol-accelerated degradation of the membrane domain of hamster 3-hydroxy-3-methylglutaryl-coenzyme A reductase in insect cells. *J. Biol. Chem.* **284,** 26778–26788
6. Lange, Y., Ory, D. S., Ye, J., Lanier, M. H., Hsu, F. F., and Steck, T. L. (2008) Effectors of rapid homeostatic responses of endoplasmic reticulum cholesterol and 3-hydroxy-3-methylglutaryl-CoA reductase. *J. Biol. Chem.* **283,** 1445–1455
7. Song, B. L., Sever, N., and DeBose-Boyd, R. A. (2005) Gp78, a membrane-anchored ubiquitin ligase, associates with Insig-1 and couples sterol-regulated ubiquitination to degradation of HMG CoA reductase. *Mol. Cell* **19,** 829–840
8. Jo, Y., Lee, P. C., Sguigna, P. V., and DeBose-Boyd, R. A. (2011) Sterol-induced degradation of HMG CoA reductase depends on interplay of two Insigs and two ubiquitin ligases, gp78 and Trc8. *Proc. Natl. Acad. Sci. U.S.A.* **108,** 20503–20508
9. Morris, L. L., Hartman, I. Z., Jun, D. J., Seemann, J., and DeBose-Boyd, R. A. (2014) Sequential actions of the AAA-ATPase valosin-containing protein (VCP)/p97 and the proteasome 19 S regulatory particle in sterol-accelerated, endoplasmic reticulum (ER)-associated degradation of 3-hydroxy-3-methylglutaryl-coenzyme A reductase. *J. Biol. Chem.* **289,** 19053–19066
10. Horton, J. D., Shah, N. A., Warrington, J. A., Anderson, N. N., Park, S. W., Brown, M. S., and Goldstein, J. L. (2003) Combined analysis of oligonucleotide microarray data from transgenic and knockout mice identifies direct SREBP target genes. *Proc. Natl. Acad. Sci. U.S.A.* **100,** 12027–12032
11. Yang, T., Espenshade, P. J., Wright, M. E., Yabe, D., Gong, Y., Aebersold, R., Goldstein, J. L., and Brown, M. S. (2002) Crucial step in cholesterol homeostasis: sterols promote binding of SCAP to INSIG-1, a membrane protein that facilitates retention of SREBPs in ER. *Cell* **110,** 489–500
12. Yabe, D., Brown, M. S., and Goldstein, J. L. (2002) Insig-2, a second endoplasmic reticulum protein that binds SCAP and blocks export of sterol regulatory element-binding proteins. *Proc. Natl. Acad. Sci. U.S.A.* **99,** 12753–12758
13. Feramisco, J. D., Goldstein, J. L., and Brown, M. S. (2004) Membrane topology of human insig-1, a protein regulator of lipid synthesis. *J. Biol. Chem.* **279,** 8487–8496
14. Yabe, D., Komuro, R., Liang, G., Goldstein, J. L., and Brown, M. S. (2003) Liver-specific mRNA for Insig-2 down-regulated by insulin: implications for fatty acid synthesis. *Proc. Natl. Acad. Sci. U.S.A.* **100,** 3155–3160
15. Summons, R. E., Bradley, A. S., Jahnke, L. L., and Waldbauer, J. R. (2006) Steroids, triterpenoids and molecular oxygen. *Philos. Trans. R. Soc. Lond B. Biol. Sci.* **361,** 951–968
16. Bloch, K. (1952) Biological synthesis of cholesterol. *Harvey Lect.* **48,** 68–88
17. Nguyen, A. D., McDonald, J. G., Bruick, R. K., and DeBose-Boyd, R. A. (2007) Hypoxia stimulates degradation of 3-hydroxy-3-methylglutaryl-coenzyme A reductase through accumulation of lanosterol and hypoxia-inducible factor-mediated induction of insigs. *J. Biol. Chem.* **282,** 27436–27446
18. Semenza, G. L. (2012) Hypoxia-inducible factors in physiology and medicine. *Cell* **148,** 399–408
19. Kaelin, W. G., Jr., and Ratcliffe, P. J. (2008) Oxygen sensing by metazoans: the central role of the HIF hydroxylase pathway. *Mol. Cell* **30,** 393–402
20. Wenger, R. H., Stiehl, D. P., and Camenisch, G. (2005) Integration of oxygen signaling at the consensus HRE. *Sci. STKE* **2005,** re12
21. Jaakkola, P., Mole, D. R., Tian, Y. M., Wilson, M. I., Gielbert, J., Gaskell, S. J., von Kriegsheim, A., Hebestreit, H. F., Mukherji, M., Schofield, C. J., Maxwell, P. H., Pugh, C. W., and Ratcliffe, P. J. (2001) Targeting of HIF-$\alpha$ to the von Hippel-Lindau ubiquitylation complex by $O_2$-regulated prolyl hydroxylation. *Science* **292,** 468–472
22. Haase, V. H., Glickman, J. N., Socolovsky, M., and Jaenisch, R. (2001) Vascular tumors in livers with targeted inactivation of the von Hippel-Lindau tumor suppressor. *Proc. Natl. Acad. Sci. U.S.A.* **98,** 1583–1588
23. Hwang, S., Hartman, I. Z., Calhoun, L. N., Garland, K., Young, G. A., Mitsche, M. A., McDonald, J., Xu, F., Engelking, L., and DeBose-Boyd, R. A. (2016) Contribution of accelerated degradation to feedback regulation of 3-hydroxy-3-methylglutaryl coenzyme A reductase and cholesterol metabolism in the liver. *J. Biol. Chem.* **291,** 13479–13494
24. Firth, J. D., Ebert, B. L., Pugh, C. W., and Ratcliffe, P. J. (1994) Oxygen-regulated control elements in the phosphoglycerate kinase 1 and lactate dehydrogenase A genes: similarities with the erythropoietin 3′ enhancer 115. *Proc. Natl. Acad. Sci. U.S.A.* **91,** 6496–6500
25. Wang, G. L., and Semenza, G. L. (1993) Characterization of hypoxia-inducible factor 1 and regulation of DNA binding activity by hypoxia. *J. Biol. Chem.* **268,** 21513–21518
26. Fernández-Alvarez, A., Soledad Alvarez, M., Cucarella, C., and Casado, M. (2010) Characterization of the human insulin-induced gene 2 (INSIG2) promoter: the role of Ets-binding motifs. *J. Biol. Chem.* **285,** 11765–11774
27. Zhu, J., Jiang, X., and Chehab, F. F. (2014) FoxO4 interacts with the sterol regulatory factor SREBP2 and the hypoxia inducible factor HIF2$\alpha$ at the CYP51 promoter. *J. Lipid Res.* **55,** 431–442
28. Dolt, K. S., Karar, J., Mishra, M. K., Salim, J., Kumar, R., Grover, S. K., and Qadar Pasha, M. A. (2007) Transcriptional downregulation of sterol metabolism genes in murine liver exposed to acute hypobaric hypoxia. *Biochem. Biophys. Res. Comm.* **354,** 148–153
29. Drabkin, H. A., and Gemmill, R. M. (2012) Cholesterol and the development of clear-cell renal carcinoma. *Curr. Opin. Pharmacol.* **12,** 742–750

30. Gebhard, R. L., Clayman, R. V., Prigge, W. F., Figenshau, R., Staley, N. A., Reesey, C., and Bear, A. (1987) Abnormal cholesterol metabolism in renal clear cell carcinoma. *J. Lipid Res.* **28,** 1177–1184
31. Tugnoli, V., Trinchero, A., and Tosi, M. R. (2004) Evaluation of the lipid composition of human healthy and neoplastic renal tissues. *Ital. J. Biochem.* **53,** 169–182
32. Yang, H., Minamishima, Y. A., Yan, Q., Schlisio, S., Ebert, B. L., Zhang, X., Zhang, L., Kim, W. Y., Olumi, A. F., and Kaelin, W. G., Jr. (2007) pVHL acts as an adaptor to promote the inhibitory phosphorylation of the NF-κB agonist Card9 by CK2. *Mol. Cell* **28,** 15–27
33. Gruenbacher, G., and Thurnher, M. (2015) Mevalonate metabolism in cancer. *Cancer Lett.* **356,** 192–196
34. Russell, D. W., Schneider, W. J., Yamamoto, T., Luskey, K. L., Brown, M. S., and Goldstein, J. L. (1984) Domain map of the LDL receptor: sequence homology with the epidermal growth factor precursor. *Cell* **37,** 577–585
35. Liang, G., Yang, J., Horton, J. D., Hammer, R. E., Goldstein, J. L., and Brown, M. S. (2002) Diminished hepatic response to fasting/refeeding and liver X receptor agonists in mice with selective deficiency of sterol regulatory element-binding protein-1c. *J. Biol. Chem.* **277,** 9520–9528
36. Engelking, L. J., Liang, G., Hammer, R. E., Takaishi, K., Kuriyama, H., Evers, B. M., Li, W. P., Horton, J. D., Goldstein, J. L., and Brown, M. S. (2005) Schoenheimer effect explained: feedback regulation of cholesterol synthesis in mice mediated by Insig proteins. *J. Clin. Invest.* **115,** 2489–2498
37. Jo, Y., Hartman, I. Z., and DeBose-Boyd, R. A. (2013) Ancient ubiquitous protein-1 mediates sterol-induced ubiquitination of 3-hydroxy-3-methylglutaryl CoA reductase in lipid droplet-associated endoplasmic reticulum membranes. *Mol. Biol. Cell* **24,** 169–183
38. Liscum, L., Luskey, K. L., Chin, D. J., Ho, Y. K., Goldstein, J. L., and Brown, M. S. (1983) Regulation of 3-hydroxy-3-methylglutaryl coenzyme A reductase and its mRNA in rat liver as studied with a monoclonal antibody and a cDNA probe. *J. Biol. Chem.* **258,** 8450–8455
39. McFarlane, M. R., Liang, G., and Engelking, L. J. (2014) Insig proteins mediate feedback inhibition of cholesterol synthesis in the intestine. *J. Biol. Chem.* **289,** 2148–2156
40. Schofield, C. J., and Ratcliffe, P. J. (2004) Oxygen sensing by HIF hydroxylase. *Nat. Rev. Mol. Cell Biol.* **5,** 343–354
41. Semenza, G. L. (2004) Hydroxylation of HIF-1: oxygen sensing at the molecular level. *Physiology* **19,** 176–182
42. Mitsche, M. A., McDonald, J. G., Hobbs, H. H., and Cohen, J. C. (2015) Flux analysis of cholesterol biosynthesis *in vivo* reveals multiple tissue and cell-type specific pathways. *eLife* **4,** e07999